

# Entropic formation of a thermodynamically stable colloidal quasicrystal with negligible phason strain

Kwanghwi Je<sup>a</sup> , Sangmin Lee (이상민)<sup>a</sup> , Erin G. Teich<sup>b,1</sup> , Michael Engel<sup>c,2</sup>, and Sharon C. Glotzer<sup>a,b,d,2</sup>

<sup>a</sup>Department of Chemical Engineering, University of Michigan, Ann Arbor, MI 48109; <sup>b</sup>Applied Physics Program, University of Michigan, Ann Arbor, MI 48109; Institute for Multiscale Simulation, Interdisciplinary Center for Nanostructured Films, Friedrich-Alexander University Erlangen-Nürnberg, 91058 Erlangen, Germany; and <sup>d</sup>Biointerfaces Institute, University of Michigan, Ann Arbor, MI 48109

Edited by David A. Weitz, Harvard University, Cambridge, MA, and approved January 9, 2021 (received for review June 8, 2020)

Quasicrystals have been discovered in a variety of materials ranging from metals to polymers. Yet, why and how they form is incompletely understood. In situ transmission electron microscopy of alloy quasicrystal formation in metals suggests an error-and-repair mechanism, whereby quasiperiodic crystals grow imperfectly with phason strain present, and only perfect themselves later into a high-quality quasicrystal with negligible phason strain. The growth mechanism has not been investigated for other types of quasicrystals, such as dendrimeric, polymeric, or colloidal quasicrystals. Soft-matter quasicrystals typically result from entropic, rather than energetic, interactions, and are not usually grown (either in laboratories or in silico) into large-volume quasicrystals. Consequently, it is unknown whether soft-matter quasicrystals form with the high degree of structural quality found in metal alloy quasicrystals. Here, we investigate the entropically driven growth of colloidal dodecagonal quasicrystals (DQCs) via computer simulation of systems of hard tetrahedra, which are simple models for anisotropic colloidal particles that form a quasicrystal. Using a pattern recognition algorithm applied to particle trajectories during DQC growth, we analyze phason strain to follow the evolution of quasiperiodic order. As in alloys, we observe high structural quality; DQCs with low phason strain crystallize directly from the melt and only require minimal further reduction of phason strain. We also observe transformation from a denser approximant to the DQC via continuous phason strain relaxation. Our results demonstrate that soft-matter quasicrystals dominated by entropy can be thermodynamically stable and grown with high structural quality—just like their alloy quasicrystal counterparts.

quasicrystal growth | tilings | colloidal crystal | entropic crystallization | phason

Quasicrystals are crystals that possess long-range quasiperiodic order without translational periodicity. Since the first report of an icosahedral quasicrystal in an Al-Mn alloy melt (1), quasicrystals with 8-, 10-, 12-, and 18-fold symmetry as well as icosahedral symmetry have been discovered in many alloys (2), carbon allotropes (3, 4), metal oxides (5), and various soft-matter systems including dendrimers (6), block copolymers (7, 8), and colloids (9-12). The apparent structural universality of quasicrystals across these very disparate systems begs the question: Is quasicrystal growth the same across all systems, regardless of length scale?

How quasicrystals form is a matter of some debate (13, 14). Two growth models have been proposed: the matching rule model and the error-and-repair model. The matching rule model (15) asserts that quasicrystals form as tiles—i.e., subunits of the quasicrystal pattern comprising clusters of particles in specific arrangements—attach at the growth front to match the existing pattern. Matching rules dictate which attachments are allowed and which are not, and the model imagines that the tiles act as puzzle pieces with precise local fit. Via matching rules, quasicrystals grow "perfectly," maintaining strict quasiperiodicity at all times, thereby resulting in an ideal (or perfect) tiling. In contrast, the error-and-repair model (16, 17) describes quasicrystal formation as a two-step process. In the first step, tiles or particle clusters quickly attach to the growing quasicrystal in a way that is at least to some degree random. These imperfect attachments eventually produce phason strain, a measure of quasiperiodic disorder over long distances (18, 19). In the second—much slower-step, phason strain is relaxed through local particle rearrangements called phason flips. Ultimately, a quasicrystal with negligible phason strain is possible, so that the end result for both models can be very similar.

Recent in situ observations of decagonal (10-fold) quasicrystal growth from Al-Ni-Co melts using transmission electron microscopy (17) and of a self-assembling icosahedral quasicrystal using molecular dynamics simulations from a single-particle species interacting via an isotropic pair potential (20) support the error-and-repair mechanism. While these two systems, one experimental and one computational, are clearly different, in both cases potential energy, rather than entropy, drives quasicrystal growth. Which growth model holds for entropically driven quasicrystal formation (21-23)? There is recent evidence that kinetic crystallization pathways in energy-dominated and entropy-dominated systems are similar (24). Does it follow that soft-matter quasicrystals form via error-and-repair, and thus that high-quality quasicrystals are realizable in entropy-driven soft-matter systems?

In this work, we answer this question for the case of the dodecagonal quasicrystal (DQC) in the hard tetrahedron system (25). Because the tetrahedron particles are hard, i.e., interact only via excluded volume, the system we study is governed solely

## **Significance**

Quasicrystals—ordered crystals lacking translational periodicity occur in systems comprising building blocks ranging from atoms to nanoparticles. These quasicrystals can have the same structure despite the obvious differences in building-block type or size. Do they all form in the same way? Or do colloidal quasicrystals grow differently than atomic quasicrystals? We study the formation of a colloidal quasicrystal in a hard tetrahedron system, where structural ordering is solely governed by entropy. We observe that the colloidal quasicrystal forms with high structural quality when simulations begin in the melt. We also find that structural imperfections in approximant crystals can be repaired by the relaxation process observed during quasicrystal formation. This demonstrates that our quasicrystal is thermodynamically stable.

Author contributions: K.J., M.E., and S.C.G. designed research; K.J., S.L., E.G.T., M.E., and S.C.G. performed research; K.J. contributed new reagents/analytic tools; K.J. analyzed data; and K.J., M.E., and S.C.G. wrote the paper.

The authors declare no competing interest

This article is a PNAS Direct Submission.

Published under the PNAS license

<sup>1</sup>Present address: Department of Bioengineering, University of Pennsylvania, Philadelphia, PA 19104.

<sup>2</sup>To whom correspondence may be addressed. Email: michael.engel@fau.de or sglotzer@

This article contains supporting information online at https://www.pnas.org/lookup/suppl/ doi:10.1073/pnas.2011799118/-/DCSupplemental.

Published February 9, 2021.

Downloaded from https://www.pnas.org by 99.110.79.82 on July 27, 2022 from IP address 99.110.79.82.

by entropy—that is, the DQC forms from entropy maximization and thus is a good representation of a soft-matter quasicrystal. We discover from Monte Carlo (MC) simulation runs that phason strain remains small during DQC growth and only weakly relaxes further, resulting in a high-quality DQC with negligible phason strain directly from the melt. We also observe that an approximant structure, a periodic crystal closely resembling the DOC and with inherent linear phason strain (25, 26), can relax to the DQC via continuous phason strain relaxation; that is, the solid-solid transition (27, 28) occurs via a process analogous to the repair step of the error-and-repair model (16, 17).

### Results

Tiling Hierarchy. Phason strain analysis is best performed by considering the tiling patterns for the quasicrystal under study. Fig. 1A introduces a hierarchical series of four tilings. All tilings are generated by inflation or deflation (2) with inflation factor  $f = 2\cos(\pi/15) \approx 1.956$  to rescale the tile edge length. At each hierarchy level, the centers of vertex motifs (Fig. 1B) form vertices of square, triangle, and rhombus tiles. The tiling employed in previous work (25) corresponds to the third hierarchy level (red color in Fig. 1B), in which clusters of 22 tetrahedra are arranged in a noninterdigitating fashion; that is, the clusters do not share tetrahedra. A single 22-tetrahedron cluster (22-T) consists of a ring of 12 tetrahedra and 2 pentagonal dipyramids (SI Appendix, Fig. S1) (25).

Phason strain in quasicrystals is quantified by numerically evaluating the geometry of the tiling. This analysis is independent of the tiling chosen within the series up to linear scaling. This means the DQC structure can in principle be analyzed using any of the four tilings in Fig. 1. The second hierarchy level (green color in Fig. 1B) is used in the present work. Details on tile decorations are shown in *SI Appendix*, Fig. S2.

Growth of the Quasicrystalline Tiling. As an initial step, we investigate the appearance of densely packed local motifs that are involved in the formation of various quasicrystals including DQCs (29–32). In dense fluid of hard tetrahedra, three local motifs have been identified: the pentagonal dipyramid (PD), icosahedron, and 22-T (SI Appendix, Figs. S3 and S4). We investigate the evolution of these motifs along the DQC assembly

pathway obtained from an MC simulation initialized in a dense fluid phase at constant packing fraction  $\phi = 0.49$  (Fig. 24). At this packing fraction, previous work has shown that fluid-DQC coexistence is thermodynamically preferred (25). After  $8 \times 10^6$ MC sweeps, the fraction of tetrahedra belonging to a 22-T motif significantly increases, while the fraction of tetrahedra belonging to the icosahedron and/or PD motifs only decreases. In the late stages of the simulation, 22-T becomes the dominant motif. In parallel with this, the local density distribution gradually evolves from unimodal to bimodal by growing a second, high-density peak (Fig. 2B). Both observations indicate that quasicrystal nucleation occurs at  $8 \times 10^6$  MC sweeps and that the motif involved in nucleation and growth in the hard tetrahedron system is the 22-T (Movie \$1).

We can obtain an intuitive picture of the contribution of 22-Ts to DQC formation by considering their spatial arrangements in the dense fluid. For this, we identify clusters of particle-sharing 22-Ts. Specifically, we track the clusters that comprise 22-Ts with six or more neighboring 22-Ts (SI Appendix, Fig. S5). As shown in SI Appendix, Fig. S6A, relatively small clusters emerge and disappear in the fluid in the early stages of the simulation trajectory (before nucleation). After  $8 \times 10^6$  MC sweeps (postnucleation), a single large cluster emerges (SI Appendix, Fig. S6B and Movie S2). The diffraction pattern of the growing cluster exhibits 12-fold symmetry (Fig. 2C), indicating that the cluster is growing as a DQC. More discussion on the self-assembly of the DQC is provided in SI Appendix, Figs. S7 and S8.

The 22-T motifs in the growing cluster form square, triangle, and rhombus tiles as demonstrated by the networks of 22-T centers (green solid circles) in Fig. 2D (SI Appendix, Fig. S9 and Movie S3). Diffraction patterns and bond orientational order diagrams of the 22-T centers in the growing cluster also show 12-fold symmetry (Fig. 2D and SI Appendix, Fig. S9B) with sharpening peaks, confirming that the evolving arrangements of the tiles correspond to a growing DQC tiling.

Analysis of Phason Strain. We calculated the phason strain in the DQC tiling during quasicrystal growth by performing a phason displacement field analysis (11, 20, 33). For this purpose, we prepared a large DQC in a thin tetragonal box by seed-assisted growth with N = 129,030 hard tetrahedra. The 12-fold axis of the

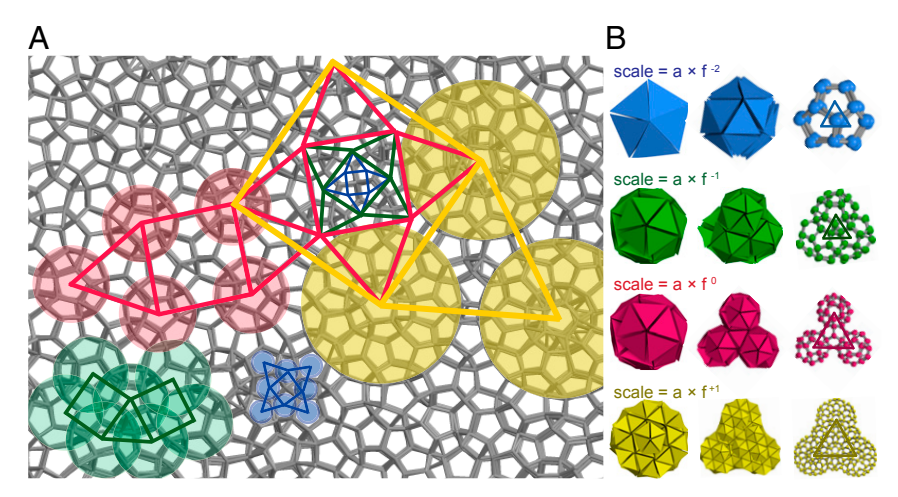


Fig. 1. Tilling hierarchy in the DQC from hard regular tetrahedra. (A) Thick gray lines connect the centers of nearest-neighbor tetrahedra. The DQC can be described as a decorated tiling on different hierarchy levels as indicated by colors. On each hierarchy level, tile vertices are located at the centers of motifs marked by translucent colored circles. Connecting tile vertices gives square tiles, triangle tiles, and rhombus tiles (as phason defects (50, 51), SI Appendix, Fig. 52) arranged into a quasiperiodic tiling. Four hierarchical tilings are shown within the yellow square tile. (B) Left column: PD (blue), interdigitating 22-T (green), noninterdigitating 22-T (red), and large dodecahedral cluster (yellow) motifs. Middle and right columns: Arrangement of the motifs and relationship to the tetrahedron network for a triangle tile. In this work, we analyze the DQC using the green scale.

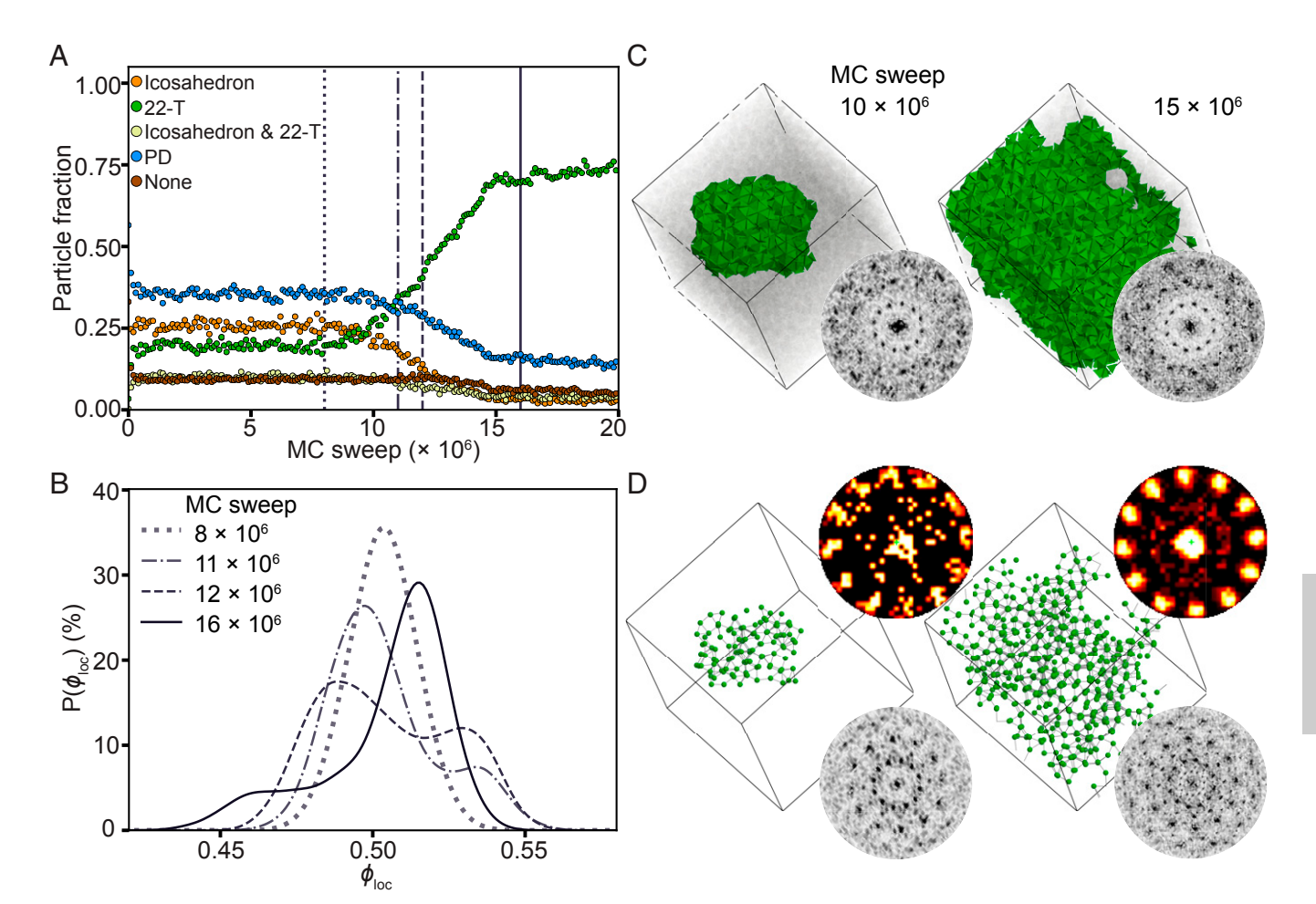


Fig. 2. Evolution of the quasicrystalline tiling during DQC growth. (A) Fractions of tetrahedra that are part of an icosahedron, a 22-T, both an icosahedron and a 22-T, a PD but not an icosahedron or a 22-T, and none of these motifs ("None") during DQC growth. All five labels add up to 100% (SI Appendix, Fig. S4). (B) Distribution of local density  $\phi_{loc}$  sampled at four different MC checkpoints as marked by the four vertical lines in A. The distribution changes from unimodal to bimodal and back to mostly unimodal, indicating first the appearance and then the partial disappearance of solid–fluid coexistence. Because the simulation is conducted in the isochoric ensemble at  $\phi = 0.49$ , peaks shift toward lower densities as the solid grows. (C) The growing solid is identified by clustering 22-Ts that share tetrahedra as shown after  $10 \times 10^6$  and  $15 \times 10^6$  MC sweeps. Tetrahedra belonging to the fluid are translucent gray. Diffraction patterns of the solid (Lower Right Inset) exhibit 12-fold symmetry indicating that the solid is a DQC. (D) Networks of 22-T centers in C, which define the quasicrystalline tiling of DQC (green hierarchy level in Fig. 1). Spots in bond orientational order diagrams (Upper Right Inset) and diffraction patterns (Lower Right Inset) of the tilings gradually sharpen as DQC growth proceeds.

seed was aligned parallel to the short box axis such that growth of the 12-fold tiling proceeded laterally (see *Materials and Methods* for more details). We find that it is important to not restrict phason strain relaxation by periodic boundary conditions. For this reason, we performed the simulation at constant packing fraction  $\phi = 0.47$ , which corresponds to a density at which the DQC coexists with its fluid. In this way, the DQC does not grow into itself across periodic boundaries and is always surrounded by fluid. The contact with the fluid allows the quasicrystal to continuously relax its phason strain and reach thermodynamic equilibrium.

Downloaded from https://www.pnas.org by 99.110.79.82 on July 27, 2022 from IP address 99.110.79.82.

For the phason displacement analysis, each vertex  $a_m$  of the two-dimensional (2D) tiling is assigned to a point in a four-dimensional (4D) configurational space by a lifting procedure (*SI Appendix*). The lifted 4D point is then projected onto the phonon-corrected position of the vertex  $a_m^{\parallel}$  in 2D parallel space and a coordinate in 2D perpendicular space  $a_m^{\perp}$  that encodes phason displacement (*SI Appendix*) (34). The relationship of the distance between two tile vertices in parallel space,  $r_m^{\parallel} = |a_m^{\parallel} - a_n^{\parallel}|$ , and the corresponding distance in perpendicular

space,  $r_{mn}^{\perp} = \left| a_m^{\perp} - a_n^{\perp} \right|$  characterizes phason strain and is defined as the phason displacement (*SI Appendix*) (33). In particular, the slope  $\alpha$  of the linear fit,  $r^{\perp} = \alpha r^{\parallel} + \beta$  is known as the phason strain (*SI Appendix*) (35). We calculate  $\alpha$  after removing background noise (*SI Appendix*, Fig. S10) and scale  $\alpha$  by the value of phason strain in the first-order approximant (*SI Appendix*) (25, 26)  $\alpha_{1st}$ .

Fig. 3A shows a growing DQC (first row) and its corresponding quasicrystalline tiling (second row). DQC growth is complete after approximately  $9 \times 10^6$  MC sweeps, which is reflected in the convergence of the reduced pressure  $P^* = P/k_BT$  (magenta arrowhead in Fig. 3B) and that of the fraction of particles belonging to the solid (SI Appendix, Fig. S11). At  $9 \times 10^6$  MC sweeps, the phason strain is  $\alpha/\alpha_{1st} = 0.013$  (green arrow in Fig. 3 B and C), which is comparable to the phason strain in the third-order approximant of the DQC (SI Appendix) (25),  $\alpha_{3rd}/\alpha_{1st} = 0.010$  (SI Appendix, Fig. S12). The phason strain then gradually decreases, becoming negligible (zero) at around  $18 \times 10^6$  MC sweeps (cyan arrow in Fig. 3 B and C). These results demonstrate that only weak phason strain is introduced during

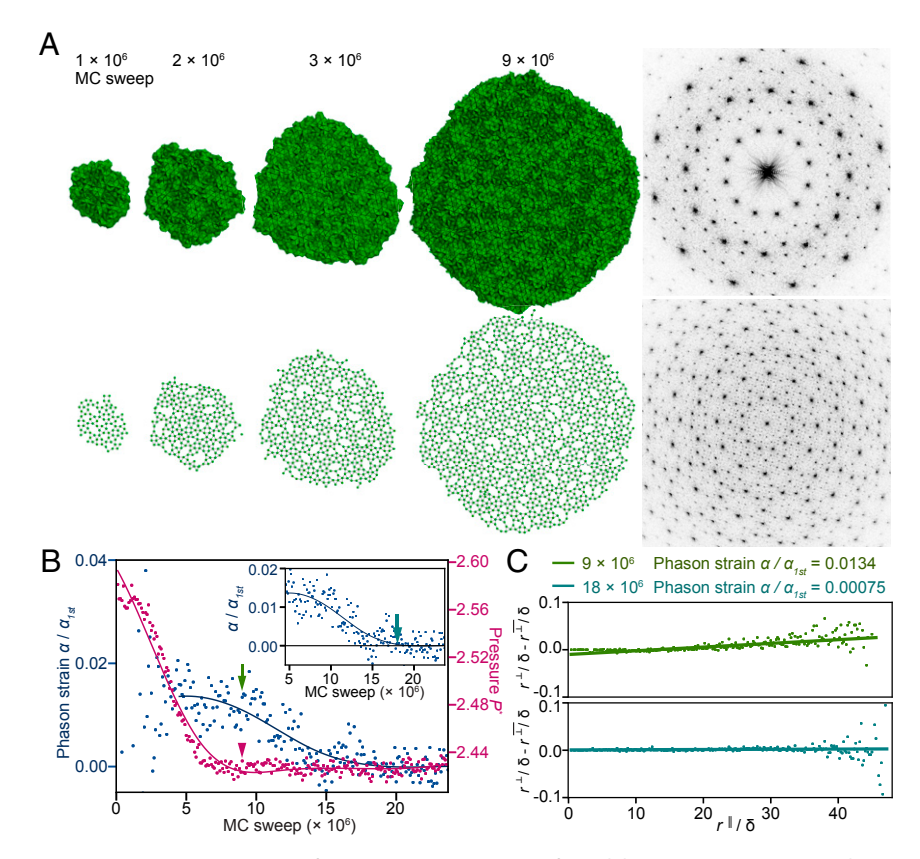


Fig. 3. Phason strain analysis during DQC growth starting from the hard tetrahedron fluid. (A) The growing DQC solid (*Upper Row*) and its tiling (*Lower Row*). Diffraction patterns at  $9 \times 10^6$  MC sweeps for tetrahedron centers (*Upper Right*) and tiling vertices (*Lower Right*) show many peaks with 12-fold symmetry, indicating a well-formed quasicrystal. (B) Evolution of system pressure P\* (magenta) and phason strain  $\alpha$  measured from the tiling (blue). The tiling size is large enough to measure phason strain reliably after  $4.5 \times 10^6$  MC sweeps (start of interpolation). Pressure converges after  $9 \times 10^6$  MC sweeps (magenta arrow). Phason strain converges more slowly after  $18 \times 10^6$  MC sweeps (*Inseet*). (C) Phason displacement field analysis at the times when pressure (green) and phason strain (cyan) each converge to equilibrium values. Here, the times are marked by green and cyan arrows in B, respectively. Phason displacement is the average perpendicular space distance  $r^{\perp}/\delta$  as a function of parallel space distance  $r^{\parallel}/\delta$ , where  $\delta$  is the tile edge length. Phason displacement grows linearly. The slope of this growth is the phason strain  $\alpha$ , which is measured from  $r^{\perp}(r^{\parallel})/\delta$  after removing background noise  $\overline{r^{\perp}}(r^{\parallel})/\delta$  (*SI Appendix*, Fig. S11) and is scaled by phason strain of the first-order approximant  $\alpha_{1st}$ . Further details are found in *SI Appendix*.

growth and subsequent relaxation eventually results in a high-quality DQC with negligible phason strain and weak equilibrium phason fluctuations (*SI Appendix*, Fig. S13 *A* and *B*). We confirm formation of high-quality DQCs with negligible phason strain in three independent simulations (*SI Appendix*, Fig. S14). More discussion on the phason strain relaxation in our DQC is provided in *SI Appendix*. Next, we show that the observed phason relaxation can even occur in quasicrystal approximants with inherent phason strain, which demonstrates thermodynamic stability of DQCs over the approximants.

Transformation of the First-Order Approximant. Quasicrystal approximants are characterized by linear phason strain (36). Lower free energy of the quasicrystal compared to its approximants is a prerequisite for thermodynamic stability of the quasicrystal and has thus been investigated in both experiment (37) and simulation (38). Specifically, the first-order DQC approximant was tested for relative stability with respect to DQC in the hard tetrahedron system (26). Equations of state demonstrated that the first-order approximant is more densely packed than both the DQC and higher-order approximants (26). These results suggested that the first-order approximant is the thermodynamically stable phase. But, no tests of its stability have been reported.

We revisited the stability of the DQC by initializing a simulation from the first-order approximant (*SI Appendix*, Fig. S20) (25, 26) in a tetragonal box at packing fraction  $\phi = 0.47$ . We now

find that the approximant gradually transforms into the DQC. This is demonstrated by the evolution of the diffraction pattern from 4-fold symmetry to 12-fold symmetry (Fig. 4A and SI Appendix, Figs. S15 and S16 and Movie S4). The transformation is also observed at a lower packing fraction  $\phi = 0.46$  (SI Appendix, Fig. S17). These results indicate that the DQC is thermodynamically more stable than approximants at these packing fractions. We confirmed that the geometry of the simulation box does not affect the transformation (SI Appendix, Fig. S18).

We calculated phason strain during the transformation using the phason displacement field analysis. The phason strain decays exponentially as  $\alpha/\alpha_{1st} \propto \exp(-t/t_0)$  with  $t_0 = 14 \times 10^6$  as a function of MC sweeps t. Phason strain is zero within fluctuations after  $t = 80 \times 10^6$  (Fig. 4B). Both types of simulations, growth from the fluid and transformation of the approximant, converge to a high-quality DQC free of phason strain, demonstrating unambiguously the thermodynamic stability of the DQC. This is an observation of a transformation from an approximant to a quasicrystal in a three-dimensional (3D) simulation and the demonstration of thermodynamic stability of a simulated DQC in 3D. Our observation is in line with previous simulation reports of entropically stabilized dodecagonal or decagonal quasicrystals in 2D (38–40).

Relaxation of phason strain requires coherent phason flips within the tiling. We analyzed the enhancement of structural quality of the tiling by following the evolution of the spatial distribution of

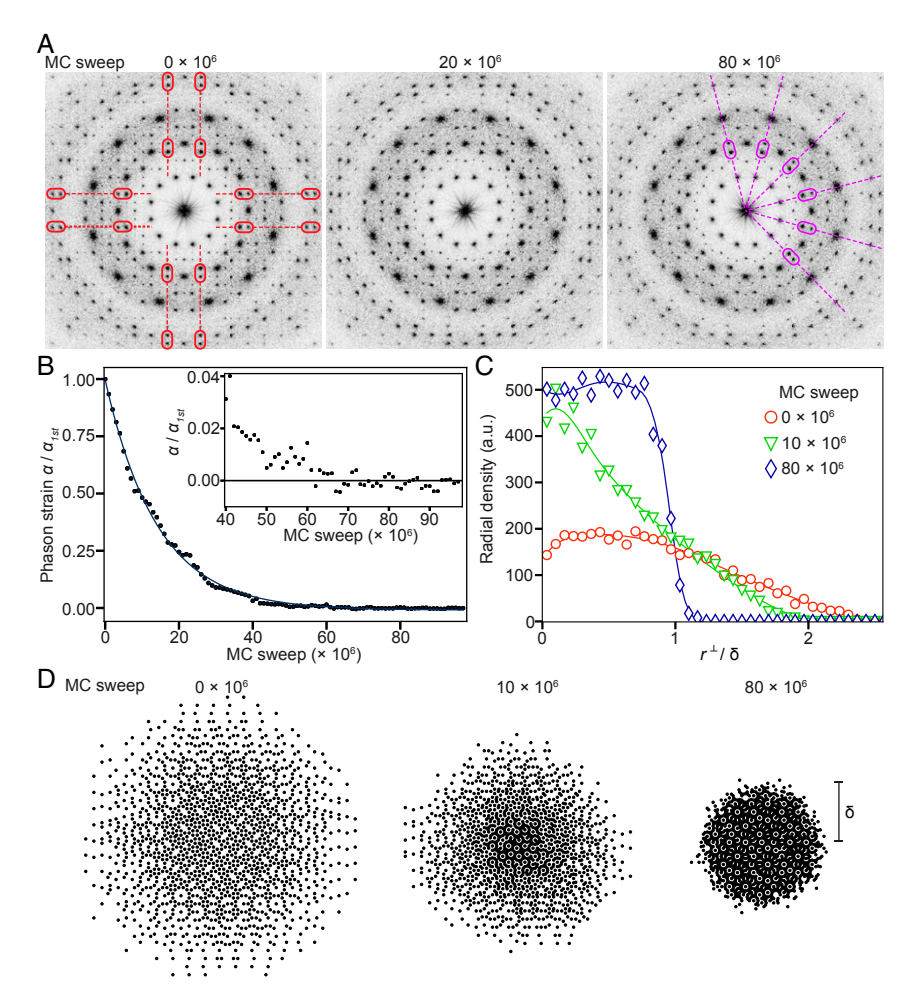


Fig. 4. Continuous transformation from the first-order approximant to the DQC during a long MC simulation. (A) Evolution of the diffraction pattern from fourfold symmetry in the approximant (0×10<sup>6</sup> MC sweeps) to 12-fold symmetry in the DQC (80×10<sup>6</sup> MC sweeps). (B) Phason strain  $\alpha/\alpha_{1st}$  gradually relaxes to zero during the transformation. (C) Radial density in perpendicular space  $r^{\perp}$  sharpens over time toward a compact occupation domain as expected for a high-quality DQC. (D) Snapshots of projected tile vertices in the perpendicular space sampled at 0×10<sup>6</sup>, 10×10<sup>6</sup>, and 80×10<sup>6</sup> MC sweeps. When the transformation is complete (80×10<sup>6</sup> MC sweeps), the positions form a single roughly circular domain with radius δ, where δ is the tile edge length. Due to random phason fluctuations, the boundary of the domain is blurred.

tile vertices projected to perpendicular space. This distribution is known as the occupation domain. It is a polygonal domain with sharp boundaries for an ideal dodecagonal tiling with shield tiles, a spherical domain blurred out near the boundary in the case of a random tiling, and a noncompact domain in the case of an approximant (33). During transformation from the approximant to the DQC, the radial density of projected points in perpendicular space gradually sharpens (Fig. 4 C and D), showing improvement in the structural quality of the tiling. The occupation domain remains blurred near the boundary, indicating that the DQC permits weak random phason fluctuations in equilibrium (SI Appendix, Fig. S13 C and D).

## Discussion

Since 2004 a growing number of colloidal quasicrystals have been reported (6–12), including a quasicrystal comprising tetrahedron-shaped nanoparticles (41). But, the quasicrystals in these systems are characterized by relatively low structural quality when compared to that of classic examples of quasicrystals of atomic alloys (2, 42). This leads to the question of whether soft-matter quasicrystals are necessarily of inferior structural quality. The purely entropic hard tetrahedron system studied in this paper can be considered a soft-matter system because the particles interact

weakly (i.e., not at all) compared to atoms. Our observation of the formation of high-quality DQCs with negligible phason strain demonstrates that soft-matter quasicrystals can indeed exhibit a high degree of quasiperiodic order comparable to their alloy counterparts. Our work also reveals a potential limiting factor toward quasicrystals with high structural quality: the need to anneal the quasicrystal long enough to heal out phason strain and other defects created initially during rapid growth. Atoms in alloys move orders of magnitude faster than the much more massive colloids, which explains why annealing is less of an issue in traditional QCs. Future work should search for formation modes that lead to softmatter quasicrystals with few defects (43) or defects that heal quickly. Those soft-matter quasicrystals will be the best candidates for functional materials, e.g., complete photonic bandgap materials for next-generation optical devices (44, 45) made via self-assembly.

#### **Materials and Methods**

**Particle Geometry.** A tetrahedron is the convex hull of the four vertices  $v_1 = (1,1,1), v_2 = (1,-1,-1), v_3 = (-1,1,-1), v_4 = (-1,-1,1)$ . Edge length and volume of the tetrahedra are  $\sigma = 2\sqrt{2}$  and V = 8/3, respectively.

**Simulation Code.** Simulations were performed with the hard-particle MC (HPMC) (46) simulation code implemented in the HOOMD-blue software package, version 2.4.2 (47). We used HPMC on multiple central processing

units (CPUs) with message passing interface domain decomposition or on a single graphics processing unit at XSEDE (48). All simulations were performed in the isochoric ensemble with periodic boundary conditions. The open-source analysis package *freud* (49) was used to detect motifs via pattern recognition and to quantify the local density distribution of tetrahedra.

**Self-Assembly Simulation.** Simulations were started from a fluid of 16,384 hard tetrahedra at low density, compressed to either packing fraction  $\phi = 0.49$  or  $\phi = 0.52$ , and run for  $20 \times 10^6$  MC sweeps.

Analysis of Local Motifs. Positions and orientations of tetrahedra were averaged over short trajectories to reduce noise. Icosahedron and 22-T motifs were detected by grouping and vector displacement analysis. In the grouping analysis, tetrahedron vertices within distance cutoff  $0.3\sigma$  were grouped. The clusters of tetrahedra containing groups of size 20 and 22 vertices are candidates for icosahedron and 22-T motifs, respectively. Subsequently, in the vector displacement analysis, we created the set of vectors connecting the center of a candidate cluster to the centers of the tetrahedra in the candidate cluster. If the angular displacements between the vector set of the candidate cluster and that of the ideal motif was lower than a threshold, the candidate motif was successfully identified with the ideal motif. Detection of PDs was performed analogously with the difference that tetrahedron edge centers instead of vertices were grouped. Local packing fraction of a tetrahedron  $\phi_{\mathrm{loc}}$  is defined as the packing fraction around the tetrahedron within a sphere of radius  $1.77\sigma$ . The local density distribution is the histogram of local packing fractions.

Seed-Assisted DQC Growth (Approximant-to-DQC Transformation) Simulations. The simulation was started from a fluid prepared by placing 129,600 (136,000) hard, regular tetrahedra at low density in a thin tetragonal simulation box and compressing the system to  $\phi=0.46$ . A static seed of 546 (50,324) hard tetrahedra was placed with the 12-fold axis of the seed pointed along the thin box dimension as shown in SI Appendix, Fig. S19 (SI Appendix, Fig. S20) and all overlapping hard tetrahedra of the fluid removed. The simulation box was then compressed to  $\phi=0.47$ . The final box dimension was  $69.3\sigma\times6.71\sigma\times69.3\sigma$  ( $70.97\sigma\times6.71\sigma\times70.97\sigma$ ). The HPMC simulation was run for  $23\times10^6(95\times10^6)$  MC sweeps with the seed immobilized for about

- D. Shechtman, I. Blech, D. Gratias, J. W. Cahn, Metallic phase with long-range orientational order and no translational symmetry. Phys. Rev. Lett. 53, 1951–1953 (1984).
- W. Steurer, S. Deloudi, Crystallography of Quasicrystals: Concepts, Methods and Structures (Springer Series in Materials Science, 2009).
- M. Paßens et al., Interface-driven formation of a two-dimensional dodecagonal fullerene quasicrystal. Nat. Commun. 8, 15367 (2017).
- S. J. Ahn et al., Dirac electrons in a dodecagonal graphene quasicrystal. Science 361, 782–786 (2018).
- S. Förster, K. Meinel, R. Hammer, M. Trautmann, W. Widdra, Quasicrystalline structure formation in a classical crystalline thin-film system. *Nature* 502, 215–218 (2013).
- 6. X. Zeng et al., Supramolecular dendritic liquid quasicrystals. Nature 428, 157–160
- K. Hayashida, T. Dotera, A. Takano, Y. Matsushita, Polymeric quasicrystal: Mesoscopic quasicrystalline tiling in ABC star polymers. Phys. Rev. Lett. 98, 195502 (2007).
- S. Fischer et al., Colloidal quasicrystals with 12-fold and 18-fold diffraction symmetry. Proc. Natl. Acad. Sci. U.S.A. 108, 1810–1814 (2011).
- D. V. Talapin et al., Quasicrystalline order in self-assembled binary nanoparticle superlattices. Nature 461, 964–967 (2009).
- C. Xiao, N. Fujita, K. Miyasaka, Y. Sakamoto, O. Terasaki, Dodecagonal tiling in mesoporous silica. *Nature* 487, 349–353 (2012).
- X. Ye et al., Quasicrystalline nanocrystal superlattice with partial matching rules. Nat. Mater. 16, 214–219 (2017).
- Y. Sun et al., Formation pathways of mesoporous silica nanoparticles with dodecagonal tiling. Nat. Commun. 8, 252 (2017).
- W. Steurer, Quasicrystal structure and growth models: Discussion of the status quo and the still open questions. J. Phys. Conf. Ser. 809, 012001 (2017).
- W. Steurer, Quasicrystals: What do we know? What do we want to know? What can we know? Acta Crystallogr. A Found. Adv. 74, 1–11 (2018).
- G. Y. Onoda, P. J. Steinhardt, D. P. DiVincenzo, J. E. S. Socolar, Growing perfect quasicrystals. *Phys. Rev. Lett.* 60, 2653–2656 (1988).
- F. Nori, M. Ronchetti, V. Elser, Strain accumulation in quasicrystalline solids. Phys. Rev. Lett. 61, 2774–2777 (1988).
- K. Nagao, T. Inuzuka, K. Nishimoto, K. Edagawa, Experimental observation of quasicrystal growth. *Phys. Rev. Lett.* 115, 075501 (2015).
- J. E. S. Socolar, T. C. Lubensky, P. J. Steinhardt, Phonons, phasons, and dislocations in quasicrystals. Phys. Rev. B Condens. Matter 34, 3345–3360 (1986).
- M. Feuerbacher, Dislocations in icosahedral quasicrystals. Chem. Soc. Rev. 41, 6745–6759 (2012).
- M. Engel, P. F. Damasceno, C. L. Phillips, S. C. Glotzer, Computational self-assembly of a one-component icosahedral quasicrystal. Nat. Mater. 14, 109–116 (2015).

 $10^6$  MC sweeps and then released. In the seed-assisted growth simulation, the DQC grows primarily in the quasiperiodic plane perpendicular to the short box axis. This approach grows a large DQC in reasonable computation time, a prerequisite to study the evolution of phason strain during the growth process. We confirmed that the short box axis does not significantly affect growth of the DQC at  $\phi = 0.47$  by performing simulations in boxes with various thicknesses (*SI Appendix*, Fig. S21).

Tiling Determination for Phason Strain Analysis. Samples were quickly compressed to  $\phi=0.64$  to remove structural noise. The DQC was set as the seed-containing tetrahedron cluster with local densities  $\phi_{\text{loc}} > 0.68$  (SI Appendix, Fig. S22). The approximant was set as the largest tetrahedron cluster with local densities  $\phi_{\text{loc}} > 0.68$ . A 2D tiling with edge length  $\delta$  was obtained by projecting the centers of interdigitating 22-T motifs onto the plane perpendicular to the 12-fold axis. Because our DQC primarily grows in the 2D quasiperiodic plane, the DQC is well described by a 2D tiling. Radial density of particle positions in perpendicular space was obtained by measuring number density in concentric rings around the center of mass.

**Data Availability.** All study data are included in the article and/or supporting information.

ACKNOWLEDGMENTS. K.J. thanks Thi Vo, Bryan VanSaders, and Joshua A. Anderson for helpful discussions. This material is based upon work supported by the US Department of Energy, Office of Science, Basic Energy Sciences, under Award DE-SC0019118 (simulations and numerical analyses). This work was also supported in part by the NSF, Division of Materials Research Award DMR 1808342 (methods and tools development). E.G.T. was supported by a University of Michigan Regents Fellowship. M.E. was supported by Deutsche Forschungsgemeinschaft through Project EN 905/4-1, the Central Institute for Scientific Computing, and the Interdisciplinary Center for Functional Particle Systems at Friedrich-Alexander University Erlangen-Nürnberg. This work used the Extreme Science and Engineering Discovery Environment (XSEDE), which is supported by NSF Grant ACI-1548562; XSEDE Award DMR 140129. This research was also supported in part through computational resources and services supported by Advanced Research Computing at the University of Michigan, Ann Arbor.

- 21. T. Dotera, Quasicrystals in soft matter. Isr. J. Chem. 51, 1197-1205 (2011).
- C. R. Iacovella, A. S. Keys, S. C. Glotzer, Self-assembly of soft-matter quasicrystals and their approximants. Proc. Natl. Acad. Sci. U.S.A. 108, 20935–20940 (2011).
- K. Barkan, H. Diamant, R. Lifshitz, Stability of quasicrystals composed of soft isotropic particles. Phys. Rev. B Condens. Matter Mater. Phys. 83, 172201 (2011).
- S. Lee, E. G. Teich, M. Engel, S. C. Glotzer, Entropic colloidal crystallization pathways via fluid-fluid transitions and multidimensional prenucleation motifs. *Proc. Natl. Acad. Sci. U.S.A.* 116, 14843–14851 (2019).
- A. Haji-Akbari et al., Disordered, quasicrystalline and crystalline phases of densely packed tetrahedra. Nature 462, 773–777 (2009).
- A. Haji-Akbari, M. Engel, S. C. Glotzer, Phase diagram of hard tetrahedra. J. Chem. Phys. 135, 194101 (2011).
- W. Steurer, Structural phase transitions from and to the quasicrystalline state. Acta Crystallogr. A 61, 28–38 (2005).
- I. Han et al., Dynamic observation of dendritic quasicrystal growth upon laser-induced solid-state transformation. Phys. Rev. Lett. 125, 195503 (2020).
- K. F. Kelton et al., First x-ray scattering studies on electrostatically levitated metallic liquids: Demonstrated influence of local icosahedral order on the nucleation barrier. Phys. Rev. Lett. 90, 195504 (2003).
- G. W. Lee et al., Link between liquid structure and the nucleation barrier for icosahedral quasicrystal, polytetrahedral, and simple crystalline phases in Ti-Zr-Ni alloys: Verification of Frank's hypothesis. Phys. Rev. B Condens. Matter Mater. Phys. 72, 174107 (2005).
- T. Dotera, T. Oshiro, P. Ziherl, Mosaic two-lengthscale quasicrystals. Nature 506, 208–211 (2014).
- T. M. Gillard, S. Lee, F. S. Bates, Dodecagonal quasicrystalline order in a diblock copolymer melt. Proc. Natl. Acad. Sci. U.S.A. 113, 5167–5172 (2016).
- T. Ishimasa, S. Iwami, N. Sakaguchi, R. Oota, M. Mihalkovič, Phason space analysis and structure modelling of 100 Å-scale dodecagonal quasicrystal in Mn-based alloy. *Philos. Mag.* 95, 3745–3767 (2015).
- A. Yamamoto, Crystallography of quasiperiodic crystals. Acta Crystallogr. A 52, 509–560 (1996).
- C. L. Henley, "Random tiling models" in Quasicrystals: The State of the Art, D. P. DiVincenzo, P. J. Steinhardt, Eds. (World Scientific, 1991), pp. 429–524.
- A. I. Goldman, R. F. Kelton, Quasicrystals and crystalline approximants. Rev. Mod. Phys. 65, 213–230 (1993).
- A.-P. Tsai, "Back to the future"—An account discovery of stable quasicrystals. Acc. Chem. Res. 36, 31–38 (2003).
- 38. A. Reinhardt, F. Romano, J. P. K. Doye, Computing phase diagrams for a quasicrystal-forming patchy-particle system. *Phys. Rev. Lett.* **110**, 255503 (2013).

- A. Kiselev, M. Engel, H.-R. Trebin, Confirmation of the random tiling hypothesis for a decagonal quasicrystal. *Phys. Rev. Lett.* 109, 225502 (2012).
- H. Pattabhiraman, A. P. Gantapara, M. Dijkstra, On the stability of a quasicrystal and its crystalline approximant in a system of hard disks with a soft corona. *J. Chem. Phys.* 143, 164905 (2015).
- Y. Nagaoka, H. Zhu, D. Eggert, O. Chen, Single-component quasicrystalline nanocrystal superlattices through flexible polygon tiling rule. *Science* 362, 1396–1400 (2018).
- 42. A.-P. Tsai, Discovery of stable icosahedral quasicrystals: Progress in understanding structure and properties. *Chem. Soc. Rev.* 42, 5352–5365 (2013).
- C. V. Achim, M. Schmiedeberg, H. Löwen, Growth modes of quasicrystals. Phys. Rev. Lett. 112, 255501 (2014).
- M. E. Zoorob, M. D. B. Charlton, G. J. Parker, J. J. Baumberg, M. C. Netti, Complete photonic bandgaps in 12-fold symmetric quasicrystals. *Nature* 404, 740–743 (2000).

- 45. Z. V. Vardeny, A. Nahata, A. Agrawal, Optics of photonic quasicrystals. *Nat. Photonics* 7, 177–187 (2013).
- J. A. Anderson, M. Eric Irrgang, S. C. Glotzer, Scalable metropolis Monte Carlo for simulation of hard shapes. Comput. Phys. Commun. 204, 21–30 (2016).
- J. A. Anderson, C. D. Lorenz, A. Travesset, General purpose molecular dynamics simulations fully implemented on graphics processing units. *J. Comput. Phys.* 227, 5342–5359 (2008).
- 48. J. Towns et al., XSEDE: Accelerating scientific discovery. Comput. Sci. Eng. 16, 62–74 (2014).
- V. Ramasubramani et al., freud: A software suite for high throughput analysis of particle simulation data. Comput. Phys. Commun. 254, 107275 (2020).
- M. Oxborrow, C. L. Henley, Random square-triangle tilings: A model for twelvefoldsymmetric quasicrystals. *Phys. Rev. B Condens. Matter* 48, 6966–6998 (1993).
- M. Heggen, L. Houben, M. Feuerbacher, Plastic-deformation mechanism in complex solids. Nat. Mater. 9, 332–336 (2010).

Downloaded from https://www.pnas.org by 99.110.79.82 on July 27, 2022 from IP address 99.110.79.82.